JOURNAL OF MATERIALS SCIENCE 32 (1997) 5817–5823

Frequency dependence of the complex impedances and dielectric behaviour of some Mg–Zn ferrites

M. H. ABDULLAH, A. N. YUSOFF
Physics Department, Faculty of Physical and Applied Sciences, Universiti Kebangsaan Malaysia, 43600 Bangi, Selangor, Malaysia

Complex impedances of some magnesium–zinc ferrites, $Mg_xZn_{1-x}Fe_2O_4$ ($x = 0.4$, 0.5, 0.6 and 0.7), in the frequency range of 1 mHz–10 MHz were measured at 300 K. The complex-plane impedance spectrum from each sample indicates that the capacitive and the resistive properties of the materials are mainly attributed to the processes that associated with the bulk (grain) and the grain boundary. A low-frequency dispersion (LFD) and a negative capacitance regions are also observed at low frequencies. A small series resistance of about the same value for all samples is also observed. The bulk and the grain boundary components are analysed by assuming a two-layer leaky capacitor. The simulated complex impedances using the Cole–Cole expression are in agreement with the measured values. The dielectric properties of the materials are attributed to the interfacial polarization and LFD at low frequencies and the orientational polarization at high frequencies. These properties result in the dielectric loss which composed of a Debye-like loss peak at high frequency end and a strong LFD below 1 Hz. Both regions exhibit universality with regard to the power-law relation between the dielectric loss (ε_r'' or χ'') and frequency as given by $\varepsilon_r'' \propto \omega^{n-1}$, where $n = 0.14$ and $n = 0.02$, respectively. The exponent is marginally negative, $n = -0.03$, in the region of negative capacitance below 3–4 mHz. The variations of the above properties and the characteristic parameters for different compositions of the Mg–Zn ferrites are discussed.

1. Introduction

Sintered ferrites are polycrystalline magnetic ceramics where various physical properties are influenced by the nature of grains (shape, size and orientation), grain boundaries, voids, inhomogeneities, surface layers and contacts. The information about the associated physical parameters of the microstructural components is important since the overall property of the materials is determined by those components. Furthermore, since the microstructure of the materials is variable from the manner in which they are prepared and treated, it is possible to reduce the unnecessary effects at least partially so that materials with improved characteristics can be obtained.

The a.c. impedance techniques have been used to study the above-mentioned characteristics in solid state electrolytes [1, 2] and ceramic oxides [3–6]. The complex-plane impedance representation is employed in separating and understanding various microstructural and external components. This is possible as the processes that associated with the individual components are usually characterized by different time constants, so that they response at different frequency ranges. Equivalent circuit models [7] have been proposed to describe the a.c. impedance of various systems in a number of different situations. In this work, measurements of complex impedance are made on an Mg–Zn ferrite system. The objectives are to study the bulk and interface phenomena as mentioned above, and also the dielectric properties of the ferrites over a wide range of frequency. It is interesting to see that various physical parameters and characteristic properties that influence the performances of the materials can be obtained and interpreted from the analysis of the complex-plane impedance spectra. Investigation of the dielectric behaviour as well as their magnetic properties is essential in the use of ferrites as the main component in electromagnetic wave absorbing and shielding materials. It is also the idea of the present work to see the status of ferrites in association with the power-law relation [8–12] for dielectric loss as a function of frequency.

2. Materials and methods

Samples of $Mg_xZn_{1-x}Fe_2O_4$ ($x = 0.4$, 0.5, 0.6 and 0.7) were prepared by a conventional sintering technique from high purity (5 N) powders of Fe_2O_3, MgO and ZnO. The oxides were mixed and ground thoroughly

0022–2461

in the desired stoichiometric compositions, then calcined at 1000 °C for 6 h and subsequently furnace-cooled to room temperature. The partially reacted mixture was reground and pelletized into a disc-shaped form of diameter 13 mm and thickness about 3 mm at a pressure of about 50 MPa. The pellets were sintered at 1150 °C for 20 h and then cooled slowly in the furnace to room temperature. The formation of a single phase cubic spinel structure for all compositions was confirmed from X-ray diffraction analysis (Siemens D5000 diffractometer).

The measurements of the real (Z') and imaginary (Z'') parts of the complex impedance, $Z^* = Z' - jZ''$ ($j = (-1)^{1/2}$), of the samples were made using a frequency response analyser (HFRA Model HF1255), as shown in Fig. 1. A sine wave signal was sent to the input terminal (T_i) of the HFRA and the sample from the signal generator (SG) terminal. The output (T_0) measured the output signal from the sample which was the voltage drop across a standard resistance (1 kΩ). HFRA then automatically analysed the signals from T_i and T_0 to give the phase difference (θ) between the input and the output signals, Z' and Z''. The data were represented as the plots of Z'' versus Z' by the computer.

The corresponding complex resistivity of the materials is $\rho^* = \rho' - j\rho''$, where $\rho' = Z'A/d$ and $\rho'' = Z''A/d$; A and d are the cross-sectional area and thickness of the sample. The complex conductivity is $\sigma^* = 1/\rho^* = \sigma' + j\sigma''$, where $\sigma' = \rho'/M$ and $\sigma'' = \rho''/M$, with $M = |Z^*|^2(A/d)^2$. When the alternating voltage, $V = V_0 e^{j\omega t}$, is applied across the material, the current that flows is given by $i = j\omega CV = j\omega\varepsilon_r C_0 V = j\omega(\varepsilon_r' - j\varepsilon_r'')C_0 V = j\omega(\varepsilon_r' - j\varepsilon_r'')A\varepsilon_0 V/d$, where C is the capacitance of the parallel plate capacitor with the ferrite material as the dielectric and C_0 is the free space capacitance of the capacitor. The current density in the material is $J = i/A$ and the electric field is $E = V/d$. Hence, $\sigma^* = \omega\varepsilon_0\varepsilon_r'' + j\omega\varepsilon_0\varepsilon_r'$, so that $\sigma^* = j\omega\varepsilon^*$, $\sigma' = \omega\varepsilon''$ and $\sigma'' = \omega\varepsilon'$. Therefore, $\sigma' = \omega\varepsilon'' = \rho'/M$ or $\varepsilon'' = \rho'/\omega M = (Z'A/d)/\omega M = Z'/|Z^*|^2(A/d) = Z'/\omega|Z^*|^2(A/d)$, similarly, $\sigma'' = \omega\varepsilon' = \rho''/M$ or $\varepsilon' = Z''/\omega|Z^*|^2(A/d)$. Finally, $\varepsilon_r' = \varepsilon'/\varepsilon_0$, $\varepsilon_r'' = \varepsilon''/\varepsilon_0$ and $\tan\delta = \tan(90 - \theta) = 1/\tan\theta = \varepsilon''/\varepsilon'$. The results for different compositions are represented as the plots of ε_r', ε_r'' and $\tan\delta$ versus frequency.

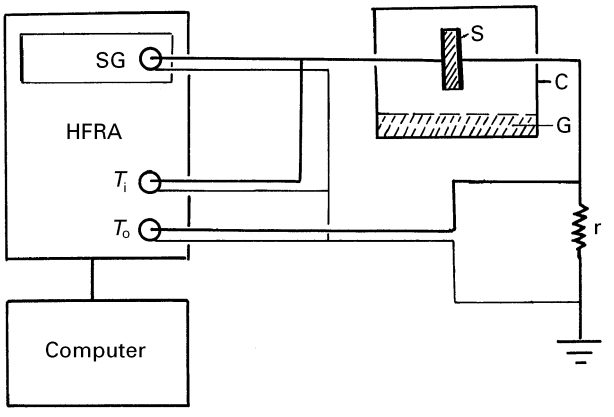

Figure 1 Experimental set-up for measuring complex impedance and phase shift by a Schlumberger HF 1255 frequency response analyser (HFRA). SG: signal generator, T_i: input terminal, T_0: output terminal, S: sample, C: glass container, G: silica gel and r: fixed resistor (1 kΩ).

3. Results and discussion

The measured complex-plane impedance spectra for the four samples are shown in Fig. 2. It can be seen that each plot shows two partially overlapping loops or semicircles covering the major part of the frequency range studied down to about 1 Hz. There is a minor segment with small but positive Z'' below 1 Hz which becomes negative below 3–4 mHz. Other features are the shift in the origin of the semicircular plots along the Z' axis and their centres are depressed to below the axis. The complex impedance data are interpreted using an equivalent circuit model in Fig. 3. The model is in the form of a two-layer Maxwell–Wagner leaky capacitor to account for the two major semicircles, with the inclusion of a resistor R_s in series to account for the shift in the origin along the Z' axis. The simulated data from the circuit, as shown in Fig. 2, are in agreement with those from the experiment. Simulation is necessary in order to ascertain the

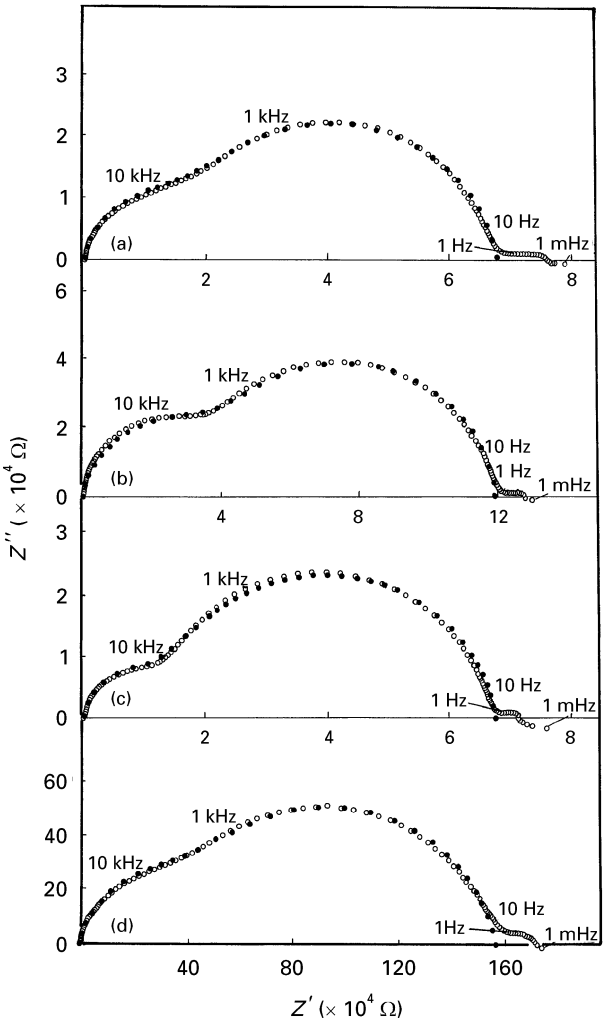

Figure 2 Complex-plane impedance spectra for $Mg_xZn_{1-x}Fe_2O_4$ ferrites at 300 K from experiment (○) and simulation (●). (a) $x = 0.4$; (b) $x = 0.5$; (c) $x = 0.6$; (d) $x = 0.7$.

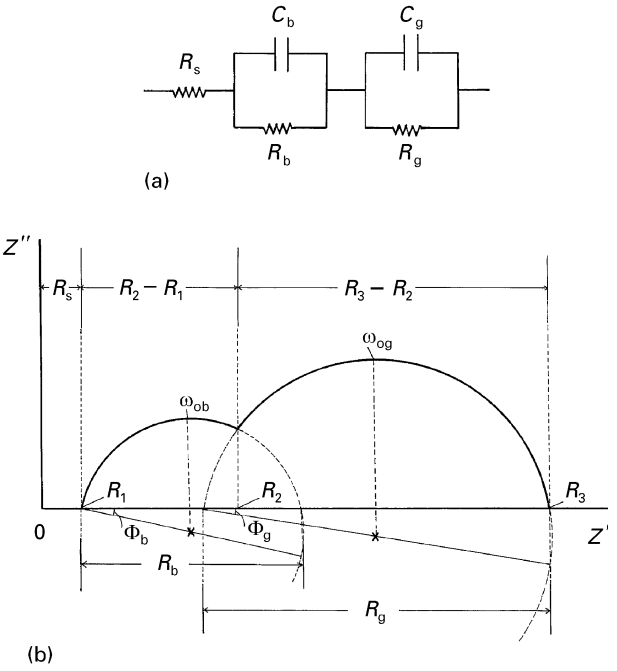

Figure 3 (a) Proposed equivalent circuit for the samples, with C_b and R_b as the probable capacitance and resistance from the bulk, C_g and R_g as the corresponding quantities from the grain boundary, and R_s the series resistance. (b) Sketch of a complex-plane impedance spectrum showing various parameters discussed in the text. ω_{ob} ($= 1/\tau_{ob}$) and ω_{og} ($= 1/\tau_{og}$) are the frequencies at the peaks of the semicircles for bulk and grain boundary.

accuracy of the calculated physical parameters that characterized the materials. The appearance of the minor segment and the negative impedance at low frequencies in the measured impedance is discussed later. The exclusion of an equivalent representation in the circuit model for the minor segment only seems to exclude its existence in the simulated impedance curve, but the agreement between the measured and simulated impedances for the rest of frequency range is maintained.

The following analysis shows that the resistances in both R–C circuits very much depend on the compositions. This indicates that both R–C circuits are the characteristic properties of the ferrite materials. The use of different materials for electrodes or holders, such as copper or stainless steel, was found to have a small effect on R_s or the shift of the spectrum along Z' axis and the minor segment at the low frequency end. On the other hand the profiles of the impedance plots that comprised the major semicircles were reproduceable. The two semicircles at high and low frequencies are identified as due to the grain or bulk (b) and grain boundary (g) phenomena respectively.

The complex impedance is presumed to obey a relation similar to the Cole–Cole expression [13] for dielectric dispersion since the frequency dependence of the complex impedance and the complex dielectric permittivity are of the same form. Thus, the Cole–Cole expression for the distribution of impedance based on the two-layer model in Fig. 3a, in which the resulting complex impedance is composed of two overlapping semicircles as in Fig. 3b, can be written as

$$Z^*(\omega) = R_s + \frac{R_2 - R_1}{1 + (j\omega\tau_{ob})^{1-\alpha_b}} + \frac{R_3 - R_2}{1 + (j\omega\tau_{og})^{1-\alpha_g}} \quad (1)$$

Hence, the real and the imaginary parts of the complex impedance are given by

$$Z'(\omega) = R_s + (R_2 - R_1)[1 + (\omega\tau_{ob})^{1-\alpha_b} \sin(\alpha_b\pi/2)]/x + (R_3 - R_2)[1 + (\omega\tau_{og})^{1-\alpha_g} \sin(\alpha_g\pi/2)]/y \quad (2a)$$

and

$$Z''(\omega) = (R_2 - R_1)[(\omega\tau_{ob})^{1-\alpha_b} \cos(\alpha_b\pi/2)]/x + (R_3 - R_2)[(\omega\tau_{og})^{1-\alpha_g} \cos(\alpha_g\pi/2)]/y \quad (2b)$$

where

$$x = 1 + (2\omega\tau_{ob})^{1-\alpha_b} \sin(\alpha_b\pi/2) + (\omega\tau_{ob})^{2(1-\alpha_b)} \quad (3a)$$

and

$$y = 1 + (2\omega\tau_{og})^{1-\alpha_g} \sin(\alpha_g\pi/2) + (\omega\tau_{og})^{2(1-\alpha_g)} \quad (3b)$$

In the above equations, $\alpha_b = 2\Phi_b/\pi$ and $\alpha_g = 2\Phi_g/\pi$, are the depression parameters which measure the deviation from the ideal Debye type of responses for the bulk and the grain boundary processes, respectively. The inclusion of α results in the tilting of the complex-plane impedance plot by $\Phi = \alpha\pi/2$. The angles of depression, Φ_b and Φ_g, for the semicircles are shown in Fig. 3. The values of α_b and α_g lie between 0 and 1 and the possible values of Φ_b and Φ_g are in the range 0 to 90°, where $\alpha_b = \alpha_g = 0$ is the case for the Debye type of impedance distribution. R_3 and R_1 are the intercepts of the impedance semicircles on the Z' axis at low and high frequencies, respectively, while R_2 is the resistance that corresponds to the projection of the point of intersection between the two semicircles onto the Z' axis. The mean relaxation times for the bulk and the grain boundary processes, $\tau_{ob} = R_bC_b$ and $\tau_{og} = R_gC_g$, are the inverse of the peak frequencies ω_{ob} and ω_{og} respectively, so that C_b and C_g can be calculated from the values of R_b and R_g.

Table I shows the calculated parameters for different compositions. The simulated complex-plane impedance spectra using Equations 2a and 2b are shown in Fig. 2. The results show that Φ_g is slightly higher than Φ_b for $x = 0.4$, 0.6 and 0.7 but equal for $x = 0.5$. It seems to be a trend toward a lower value for the two quantities at some composition between $x = 0.5$ and $x = 0.6$, although their variation with composition is small. This could be due to the effect of a significant variation in the physicochemical properties with compositions. Micrographs from a preliminary study using a scanning electron microscope (SEM) indicate that the sample $x = 0.6$ composed of fewer but larger grains compared to the sample at other compositions. This sample also indicates a higher saturation magnetization compared to others. The probable capacitances for the bulk (C_b) and the grain boundary (C_g) are in

TABLE I Magnitude of the various parameters obtained experimentally for the $Mg_xZn_{1-x}Fe_2O_4$ ferrites

	Mg content (x)			
	0.4	0.5	0.6	0.7
$R \pm 50$ (Ω)	700	700	650	750
$R_b \pm 0.05$ ($\times 10^4\ \Omega$)	2.40	5.33	1.80	60.00
$\rho_b \pm 0.05$ ($\times 10^4\ \Omega$ cm)	7.33	17.15	5.75	187.44
$R_g \pm 0.05$ ($\times 10^4\ \Omega$)	5.55	8.95	5.70	131.43
$\rho_g \pm 0.05$ ($\times 10^4\ \Omega$ cm)	17.88	28.85	18.21	410.58
$\omega_{ob} \pm 0.10$ ($\times 10^4$ rad s^{-1})	11.77	6.58	14.86	0.57
$\omega_{og} \pm 0.10$ ($\times 10^3$ rad s^{-1})	6.43	3.59	4.54	0.33
$\Phi_b \pm 0.5$ (deg.)	10.0	9.0	9.0	10.0
$\alpha_b \pm 0.01$	0.11	0.10	0.10	0.11
$\Phi_g \pm 0.5$ (deg.)	12.0	9.0	10.0	13.0
$\alpha_g \pm 0.01$	0.13	0.10	0.11	0.14
$C_b \pm 0.001$ (nF)	0.354	0.285	0.374	0.291
$C_g \pm 0.001$ (nF)	2.800	3.107	3.868	2.285
$\rho \pm 0.01$ (g cm^{-3})	4.59	4.54	5.52	4.21
$\tau_b = R_bC_b \pm 0.50$ ($\times 10^{-6}$ s)	8.49	15.19	6.73	174.72
$\tau_g = R_gC_g \pm 0.50$ ($\times 10^{-6}$ s)	15.54	278.25	220.46	3003.00

the order of 10^{-10} F and 10^{-9} F, respectively. The capacitances, C_b and C_g, are inversely proportional to the thickness of the media. The thickness of the grains is much larger than that of the grain boundaries. Thus, assuming the same order of dielectric constant for both components, the value of C_b would be smaller than that of C_g. Another feature is that C_b and C_g tend to be larger at $x = 0.6$, which means greater polarizability for the sample. The lower total resistance ($R = R_b + R_g$) at this composition promotes electron hopping, which is known to be a mechanism for both conduction and polarization in ferrites. Further consideration on the mechanism is made in the interpretation of the dielectric properties which follows.

The following discussion on dielectric properties is first aimed at interpretation of possible mechanisms for polarization, and in the latter parts the applicability of the power-law relation of the dielectric loss versus frequency and its relation with various mechanisms at different frequencies are considered. Fig. 4 shows the frequency dependence of the dielectric constant (ε_r') and dielectric loss (ε_r'') in the range of 10 mHz–10 MHz for different samples. The detailed variations of ε_r' and ε_r'' with frequency in the range of 10 kHz–10 MHz and 1 mHz–1 Hz are shown in Figs 5 and 6, respectively. The results show that the permittivities of Mg–Zn ferrites at low frequencies < 1 Hz are very high. The same order of magnitudes at the same frequencies for some ferrite materials had been discussed by previous workers [12, 13]. However, a detailed comparison on the values and trends at very low and very high frequencies cannot be made because of the lack of data at the extreme frequencies in the previous works. The results depicted in Figs 4–6 indicate the existence of more than one polarization mechanism in the materials. The loss increases sharply with decreasing frequency below 30 kHz. This behaviour of ε_r'' is normally attributed to the interfacial polarization. This type of polarization may be explained on the basis of Maxwell–Wagner two-layer

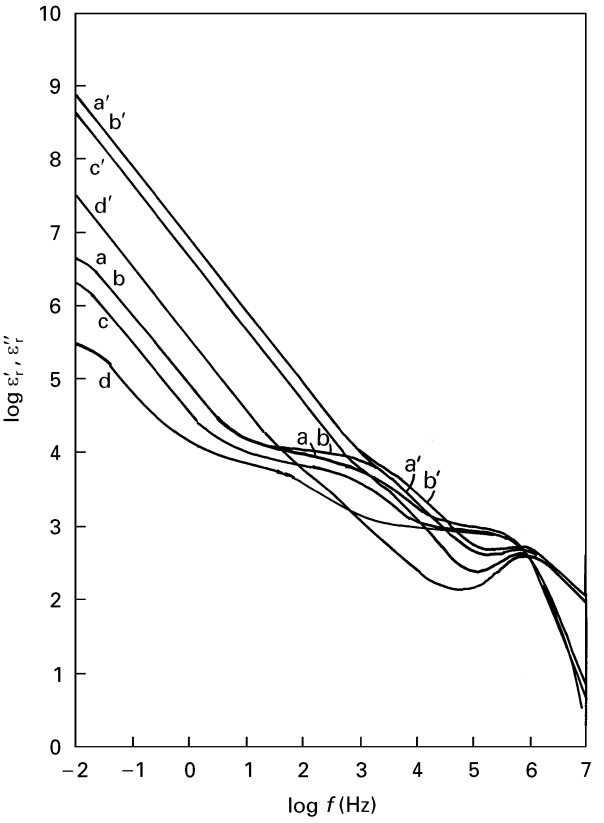

Figure 4 Plots of relative dielectric constant (ε_r') and dielectric loss (ε_r'') versus frequency in the range of 10 mHz–10 MHz for the $Mg_xZn_{1-x}Fe_2O_4$ ferrites. The experimental points are omitted for clarity. a, a′, $x = 0.4$; b, b′, $x = 0.5$; c, c′, $x = 0.6$; d, d′, $x = 0.7$.

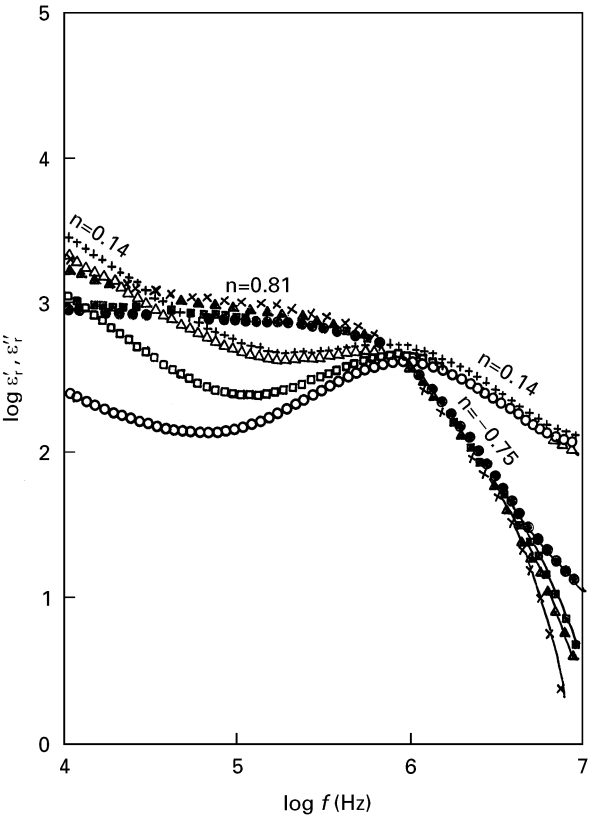

Figure 5 Plots of relative dielectric constant (ε_r' filled symbols) and dielectric loss (ε_r'' open symbols) versus frequency in the range of 10 kHz–10 MHz for the $Mg_xZn_{1-x}Fe_2O_4$ ferrites. (▲, △) $x = 0.4$; (■, □) $x = 0.5$; (×, +) $x = 0.6$; (●, ○) $x = 0.7$.

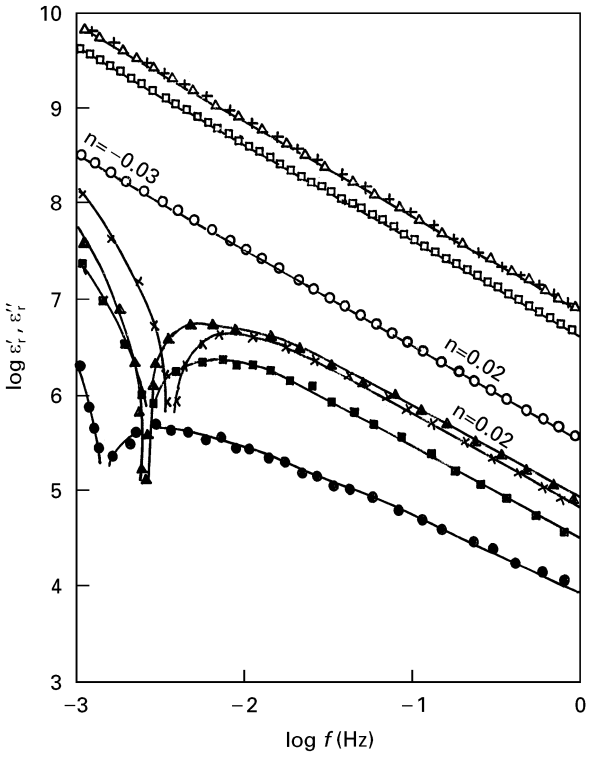

Figure 6 Plots of relative dielectric constant (ε'_r filled symbols) and dielectric loss (ε''_r open symbols) in the frequency range of 1 mHz–1 Hz. The negative dielectric constants are plotted as $\log|\varepsilon'_r|$. (▲, △) $x = 0.4$; (■, □) $x = 0.5$; (×, +) $x = 0.6$; (●, ○) $x = 0.7$.

model in a manner similar to the one for complex impedance. It is the same mechanism that results in the two associated quantities. The two-layer leaky capacitor model is an indication for the existence of interfacial polarization [16, 17]. The interfacial polarization based on the model has an additional term which is inversely proportional to the total resistance and frequency in addition to the Debye relaxation term, whereas the variation of ε'_r is similar to the Debye expression. However, the results that show both ε'_r and ε''_r rising steeply toward low frequencies may be associated with the phenomenon of low-frequency dispersion (LFD) [25]. It is thought that at frequencies < 1 Hz LFD is a dominant dielectric process in the materials. The present result shows that ε'_r for every composition tends to a maximum value on approaching 3–10 mHz, and then decreases to negative values when the frequency is further lowered. This is attributed to the appearance of negative resistance, and this property together with LFD are discussed latter in this section. The ferrites exhibit interfacial polarization due to structural inhomogenities [18]. It is thought that the hopping electrons at low frequencies may be trapped by such inhomogeneities. The results show that the interfacial polarization is dominant for frequencies below 30 kHz. The values of ε'_r and ε''_r are not decreasing continuously to zero at high frequencies as expected from the interfacial polarization . Fig. 4 shows that a behaviour analogous to the Debye relaxation process is observed at the high-frequency end. Debye relaxation is associated with dipolar materials which may experience orientational polarization in the range of 10^4–10^9 Hz. In the Debye case, ε''_r drops toward zero as the frequency is lowered. The existence of Fe^{3+} ions and the minority Fe^{2+} ions rendered ferrite materials dipolar. Fe^{2+} ions may be formed due to partial reduction of Fe^{3+} ions to Fe^{2+} ions when the ferrites were sintered at elevated temperatures. Rotational displacements of the dipoles result in the orientational polarization. In the case of ferrites, the rotation or turning of Fe^{3+}–Fe^{2+} dipoles may be viewed as the interchange of electrons between the ions so that the dipoles align themselves with the field. The potential barrier between the two types of ions will impose an inertia to the charge movement, resulting in a relaxation to the polarization process. Another possible source of orientational polarization in ferrites is the existence of cation vacancies. There is a tendency of the occupied cations to be associated with the positive ion vacancies, so that the associated pairs have dipole moments. When an electric field is applied, the cations and the vacancies in the neighbourhood can exchange positions.

Apart from the general dielectric behaviour of the four ferrite samples, as discussed above, the detailed variation of the dielectric quantities is dependent on the composition. For a fixed frequency, ε'_r decreased with increasing magnesium content, except for $x = 0.6$ which indicates otherwise. In view of Mg^{2+} and Zn^{2+} ions are of fixed charge state, it is thought that the number of the minority Fe^{2+} ion at the octahedral (B) sites that governs the polarizability in the materials. This is because of a close proximity among the Fe^{2+}/Fe^{3+} ions at the B sites compared to those at tetrahedral (A) sites. The decrease of ε'_r with Mg content is due to the reduction in the amount of Fe^{2+}/Fe^{3+} ions at the B sites upon substituting Zn^{2+} ions with Mg^{2+} ions. This is due to a tendency of a larger proportion of Mg^{2+} ions to occupy the B sites as the Mg content increased, hence transferring some Fe^{2+}/Fe^{3+} ions from B to A sites. This tendency is a consequence of the shifting of cationic distribution from normal spinel structure of zinc ferrite to the intermediate spinel structure of the magnesium–zinc ferrites. A larger ε'_r at $x = 0.6$ is consistent with a lower resistivity of the sample, and the effect is more than compensating the decrease of Fe^{2+}/Fe^{3+} ions at the B sites. A larger ε'_r also means a larger C_b, as discussed earlier. The results show that ε'_r for $x = 0.6$ are highest throughout the whole range of frequency, but very close to the values for $x = 0.4$. The trend in the compositional dependence in the interfacial region at low frequencies and in the Debye region at high frequencies is similar since both polarization processes depend on the availability of the conduction electrons, which is equal to the concentration of the Fe^{2+} ions. The essential difference is that at low frequencies in the interfacial region a large amount of electrons effectively hop between the inhomogeneities, while at high frequencies the hopping is between the Fe^{2+} and Fe^{3+} ions.

The subject of dielectric dispersion particularly dielectric loss from various experimental data has been extensively studied and reviewed [8–12, 19–26]. The main result is that the frequency dependence of the

dielectric loss of different kinds of dielectric solids follows a "universal law of loss" as given by $\varepsilon_r''(=\chi'') = B(T)\omega^{n(T)-1}$, where $B(T)$ is weakly dependent on temperature and the exponent n lies in the range $0 < n < 1$, which is shown to be typically about 0.60–0.95. It is noted that the present result also falls into a similar frequency dependence for ε_r'' but with $n = 0.14 \pm 0.01$ (slope $= -0.86$) for all samples for both the orientational Debye-like (1–10 MHz) and the interfacial region (1–10 kHz), as indicated in Fig. 5. A region of low-frequency dispersion at frequencies below 1 Hz is characterized by $n = 0.02 \pm 0.01$ (slope $= -0.98$) for both ε_r' and ε_r'', as shown in Fig. 6. The exponent for ε_r' for all samples in the Debye-like region is $n = -0.75 \pm 0.01$ (slope $= -1.75$). The value changes to $n = 0.81 \pm 0.01$ (slope $= -0.19$) on increasing the frequency to about 100 kHz. Another change of the exponent for ε_r' occurs at about 10 kHz where the value is $n = 0.19 \pm 0.01$ (slope $= -0.81$) and at 100 Hz–1 kHz with $n = 0.85 \pm 0.01$ (slope $= -0.15$). This latter change of the exponent for ε_r' within the specified range of frequency is related to relaxation of polarization in the interfacial region, as discussed earlier. The exponents for both ε_r' and ε_r'' are the same at frequencies below 1 Hz down to about 3–4 mHz where beyond this frequency ε_r' drops sharply because of the appearance of the negative capacitance.

It has been shown [20] that $n < 0.30$ is possible for nearest-neighbour interacting dipoles which is consistent with the Debye-like region, and the region of electronic hopping which is equivalent to the interfacial region. This is consistent with the proposed mechanisms discussed earlier. The power-law relation for the dielectric loss is a manifestation of the existence of a universal mechanism among different polarizable species despite the difference in the physicochemical properties of the materials. The exponent n depends on the characteristic properties of the systems but is always smaller than unity. The power-law behaviour is the outcome of many-body interaction in the dielectric relaxation processes. A small value of n and very large dielectric permittivities at low frequencies are evidence of the existence of low-frequency dispersion in the materials. However, this phenomenon is superimposed by the negative capacitance at frequencies below 3–4 mHz. In this region the exponent $n = -0.03$ (slope $= -1.03$), which is to be expected from the energy criterion [27]. From the impedance plots it can be seen that LFD corresponds to a minor segment at low frequencies, while the negative capacitance appears when the plot dips below the real Z' axis. The negative capacitance lead to negative χ' or ε_r'. The contribution of inductance, which may also lead to the negative values of both quantities, is negligible at these very low frequencies. Negative capacitance is associated with a rising current in the step-function time-domain response [27]. This effect could be due to non-linearity in the dielectric response of the ferrites at low frequencies.

It should be remarked that the Cole–Cole expression (Equation 1) is in conformity with the universal law of loss in the limit of $\omega\tau \gg 1$. In this sense

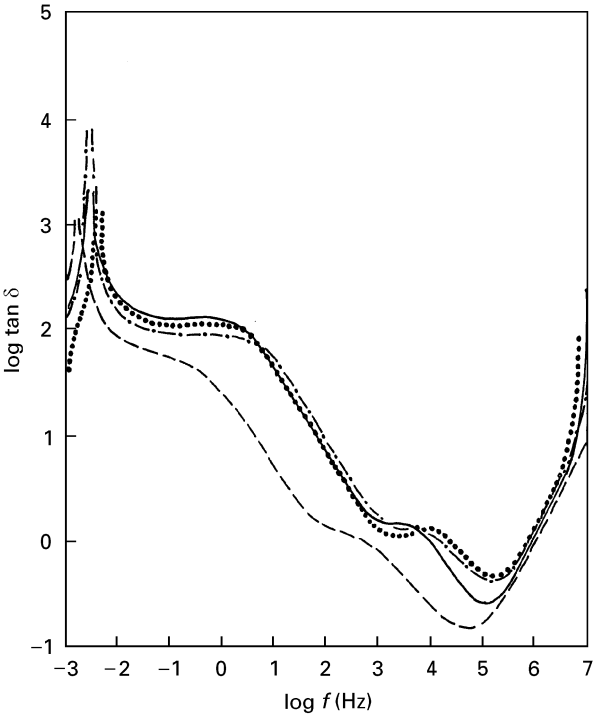

Figure 7 Frequency dependence of tan δ for the $Mg_xZn_{1-x}Fe_2O_4$ ferrites. The negative loss for each sample is plotted as log |tan δ|. (–·–) $x = 0.4$; (——) $x = 0.5$; (·····) $x = 0.6$; (---) $x = 0.7$.

$(n-1) = (\alpha-1)$ or $n = \alpha$, with both parameters lying between 0 and 1. Hence, the exponent n is in fact a fraction that measures the deviation from the ideal Debye behaviour, where $n = \alpha = 0$. Hence, the Cole–Cole expression, through equivalent circuit representation, is a useful means of analysing the a.c. impedance data. The universality in the dielectric loss is implicitly incorporated in the Cole–Cole expression through the suppression parameter. The results show that n and α(α_b and α_g in Table I), which are independently evaluated, are in a good agreement for both orientational and interfacial regions. The LFD and negative capacitance regions, which are significant at frequencies below 1 Hz, are not represented by the equivalent circuit and Cole–Cole expression. Nevertheless, their exclusion does not cause any significant error with regard to the evaluation of various physical parameters from the high-frequency processes in the materials.

Fig. 7 shows the dielectric loss $\tan\delta = \varepsilon_r''/\varepsilon_r'$ as a function of frequency. For all samples, the loss diverges at 10 MHz and just below 10 mHz at the onset of negative capacitance. There is a minimum in the loss for every sample. This occurs at a frequency that corresponds to the minimum in ε_r'', where ε_r' changes rather slowly. This is a region where ε_r' from Debye orientational polarization is predominant. Another minimum can also be seen at higher frequencies corresponds to interfacial region. The loss in the frequency range of 10 mHz–1 Hz is about constant, and this is to be expected in the region of LFD. The loss for $x = 0.7$ are significantly lower than the rest of the samples. The loss at frequency below 3–4 mHz is negative due to the negative dielectric constant.

In conclusion, the a.c. complex impedance technique is a reliable tool for studying the microstructural properties and the determination of the associated characteristic parameters of the ferrites. The technique enable the dielectric properties of the materials to be investigated as a function of frequency. The analysis of the complex impedance data through the complex-plane impedance representation and the evaluation of the dielectric permittivities provide more insights into the dielectric behaviour of the materials. The relaxations due to the interfacial and orientational polarizations and the existence of negative capacitance are the main factors that effect their dielectric behaviour. Atomic and electronic polarizations may only contribute a small constant term to the dielectric constant since the natural frequencies for atomic and electronic displacements and relaxations are in the microwave regime. It should be remarked that the Cole–Cole expression is useful in simulating the impedance plot even for a large departure from the perfect semicircular impedance distribution by combining two or possibly more semicircular arcs due to different processes. In general, the dielectric loss in the ferrites is composed of Debye-like loss peak at high frequency, interfacial loss at low frequency and a strong low-frequency dispersion at very low frequencies. All regions exhibit common feature with regard to the power-law relation between loss and frequency.

Acknowledgements

This work is supported by the Research and Development grant, IRPA 09-02-02-0005, of the Ministry of Science and Environment of Malaysia.

References

1. W. I. ARCHER and R. D. ARMSTRONG, *Electrochemistry* **7** (1979) 157.
2. S. P. S. BADWAL, in "Solid state ionic devices" (World Scientific, Singapore, 1988), p.125.
3. T. STRATON, A. MACHALE, D. BUTTON and H. L. TURNER, in "Electronic materials" edited by N. B. Hannay and U. Colombo (Plenum Press, New York, 1979) p. 71.
4. M. L. BAYARD, in "Proceedings of the International Conference on Fast Ion Transport in Solids, Electrodes and Electrolytes" 21–25 May 1979, Lake Geneva, Wisconsin (North-Holland, New York, 1979) p. 479.
5. Y. C. YEH and T. Y. TSENG, *J. Mater. Sci.* **24** (1989) 2739.
6. M. H. ABDULLAH and A. N. YUSOFF, *J. Alloys Compounds* **233** (1996) 129.
7. J. R. MACDONALD, *J. Chem. Phys.* **61** (1974) 3977, and references therein.
8. A. K. JONSCHER, *Nature* **250** (1974) 191.
9. *Idem.*, *Colloid Polym. Sci.* **253** (1975) 231.
10. *Idem.*, *Nature* **253** (1975) 717.
11. *Idem.*, *ibid.* **256** (1975) 566.
12. *Idem.*, *ibid.* **267** (1977) 673.
13. N. E. HILL, W. E. VAUGHAN, A. H. PRICE and M. DAVIES, "Dielectric properties and molecular behaviour" (Van Nostrand-Reinhold Co., New York, 1969) p. 47.
14. V. P. MIROSHKIN, V. V. PASSYNKOV and K. PERZYNSKY, *Acta Phys. Polonica* **A77** (1990) 715.
15. P. V. REDDY and T. S. RAO, *J. Less-Common Metals* **105** (1985) 63, and the references therein.
16. J. C. ANDERSON, "Dielectric" (Chapman & Hall Ltd., London, 1964) p. 96.
17. J. SEYMOUR, "Electronic devices and components" (ELBS, London, 1984) p. 421
18. S. S. SURYAVANSHI, S. R. PATIL and S. R. SAWANT, *J. Less-Common Metals* **168** (1991) 16.
19. K. L. NGAI, *Comments Solid State Phys.* **9** (1979) 127.
20. K. L. NGAI, A. K. JONSCHER and C. T. WHITE, *Nature* **277** (1979) 185.
21. K. L. NGAI and C. T. WHITE, *Phys. Rev.* **B20** (1979) 2475.
22. K. L. NGAI, *ibid.* **B22** (1980) 2066.
23. L. A. DISSADO and R. M. HILL, *Phil. Mag.* **B41** (1980) 625.
24. *Idem.*, *J. Mater. Sci.* **16** (1981) 1410.
25. A. K. JONSCHER, "Dielectric relaxation in solids" (Chelsea Dielectrics Press Ltd., London, 1983).
26. *Idem.*, *J. Mater. Sci.* **30** (1995) 2491.
27. *Idem.*, "Universal relaxation law" (Chelsea Dielectric Press Ltd., London, 1995).

Received 20 November 1995
and accepted 9 May 1997